Sphalerons at finite mixing angle

Jutta Kunz
Institute for Theoretical Physics, University of Utrecht, NL-3508 TA Utrecht, The Netherlands and Fachbereich Physik, University of Oldenburg, P.O. Box 2503, D-2900 Oldenburg, Germany

Burkhard Kleihaus
Fachbereich Physik, University of Oldenburg, P.O. Box 2503, D-2900 Oldenburg, Germany

Yves Brihaye
Department of Mathematical Physics, Mons University, Avenue Maistriau, B-7000, Mons, Belgium
(Received 18 February 1992)

The classical sphaleron is constructed for the full SU(2)×U(1) electroweak theory. Unlike the sphaleron of the SU(2) Yang-Mills-Higgs theory, it is not spherically symmetric due to the coupling to the U(1) field. It is symmetric only under rotations around the z axis and parity reflections. The mixing angle θ_W is varied over the full range $0 \leq \theta_W \leq \pi/2$. When the mixing angle is increased the energy of the sphaleron decreases, and the energy density changes its shape from a sphere at $\theta_W = 0$ to a very elongated spheroid at large values of the mixing angle. At the physical value of the mixing angle, however, the electroweak sphaleron differs only a little from the spherical sphaleron.

PACS number(s): 11.15.Kc

I. INTRODUCTION

It was observed by 't Hooft [1] that the standard model does not conserve baryon and lepton number due to Adler-Bell-Jackiw anomalies [2]. The process 't Hooft [1] considered was fermion-number violation due to instanton-induced transitions. Attracting much attention [3] Ringwald [4] recently argued that such tunneling transitions between topologically distinct vacua might indeed be observable in future accelerators.

The possibility of baryon- and lepton-number violation in the standard model was considered from another point of view by Manton [5]. Investigating the topology in the Weinberg-Salam theory, Manton showed that there are noncontractible loops in configuration space, and predicted the existence of a static, unstable solution of the field equations, a sphaleron [6], which would represent the top of the energy barrier between topologically distinct vacua.

Since at finite temperature this energy barrier between topologically distinct vacua can be overcome due to thermal fluctuations of the fields, baryon-number-violating vacuum to vacuum transitions can occur. The rate for such baryon-number-violating processes is largely determined by a Boltzmann factor, containing the height of the barrier at a given temperature and thus the energy of the sphaleron [7–10]. Baryon-number violation in the standard model due to such transitions over the barrier may be relevant for the physics of the early Universe, necessitating new scenarios for the generation of the baryon asymmetry [7–10].

In the limit of vanishing mixing angle $\theta_W = 0$ the electroweak sphaleron is well known [6,11]. In this limit the U(1) field decouples, and the energy density of the SU(2) sphaleron has spherical symmetry. At finite mixing angle the coupling to the U(1) field destroys the spherical symmetry, and the sphaleron retains only axial symmetry [6,12]. Here we consider the sphaleron of the full Weinberg-Salam theory, treating the mixing angle θ_W as a parameter, which is varied over the range $0 \leq \theta_W \leq \pi/2$.

The appropriate ansatz [12] for the axially symmetric sphaleron is analogous to the one for multimonopoles [13]. In both cases there is an Abelian gauge transformation, which preserves the structure of the ansatz [12,13]. Thus for the construction of the sphaleron a gauge-fixing condition must be chosen. In the limit $\theta_W = 0$ the sphaleron is symmetric under parity reflections. Therefore we also require parity reflection symmetry for the sphaleron at finite mixing angle [12]. (We do not consider here the "deformed" sphalerons, which appear for large Higgs-boson masses and which break this symmetry [14,15].)

In Sec. II we present the ansatz and the energy functional, and we discuss the residual Abelian gauge invariance. Because of the axial symmetry of the sphaleron at finite mixing angle, the unknown gauge and Higgs field functions entering in the ansatz depend on two variables. They represent the dynamical degrees of freedom of the system. In Sec. III we expand these functions in terms of Legendre polynomials [16,17] and solve the resulting system of coupled *ordinary* differential equations numerically. We perform the expansion up to sixth-order terms and consider the convergence of the series as a function of the weak mixing angle. In Sec. IV we solve the full system of coupled *partial* differential equations numerically and compare with the results of the expansion. We give our conclusions in Sec. V.

II. ANSATZ AND ENERGY DENSITY

Let us consider the bosonic sector of the Weinberg-Salam theory. It has the Lagrangian density

$$L=-\tfrac{1}{4}F^a_{\mu\nu}F^{a\mu\nu}-\tfrac{1}{4}f_{\mu\nu}f^{\mu\nu} +(D_\mu\Phi)^\dagger(D^\mu\Phi)-\lambda\left[\Phi^\dagger\Phi-\frac{v^2}{2}\right]^2 , \tag{2.1}$$

with the usual definitions for the SU(2) field strength tensor $F^a_{\mu\nu}$, the U(1) field strength tensor $f_{\mu\nu}$, and the covariant derivative for the Higgs field $D_\mu\Phi$.

The gauge symmetry is spontaneously broken via the Higgs potential, leading to a nonvanishing expectation value for the Higgs field,

$$\langle\Phi\rangle=\frac{v}{\sqrt{2}}\begin{bmatrix}0\\1\end{bmatrix} , \tag{2.2}$$

and the masses of gauge and Higgs bosons:

$$M_W=\tfrac{1}{2}gv,\quad M_Z=\tfrac{1}{2}\sqrt{(g^2+g'^2)}v\ ,\quad M_H=v\sqrt{2\lambda}\ . \tag{2.3}$$

The mixing angle θ_W is determined by the relation $\tan\theta_W=g'/g$, and the electric charge is $e=g\sin\theta_W$.

A. Ansatz for the axially symmetric sphaleron

Let us now consider the ansatz for the fields. Because of the coupling to the U(1) field, for finite values of the mixing angle θ_w we can require only axial symmetry around the z axis for the electroweak sphaleron. The appropriate ansatz for the fields [12] is analogous to the one discussed by Manton [13] and Rebbi and Rossi [16] for axially symmetric multimonopoles.

We define a set of orthonormal vectors

$$\begin{aligned}&\mathbf{u}_1(\phi)=(\cos\phi,\sin\phi,0) ,\\ &\mathbf{u}_2(\phi)=(0,0,1) ,\\ &\mathbf{u}_3(\phi)=(\sin\phi,-\cos\phi,0) ,\end{aligned} \tag{2.4}$$

and expand the fields as follows:

$$W^a_i(\mathbf{r})=u^j_i(\phi)u^a_k(\phi)w^k_j(\rho,z) , \tag{2.5a}$$

$$A_i(\mathbf{r})=u^j_i(\phi)a_j(\rho,z) , \tag{2.5b}$$

$$\Phi(\mathbf{r})=\tau^i u^j_i(\phi)h_j(\rho,z)\frac{v}{\sqrt{2}}\begin{bmatrix}0\\1\end{bmatrix} . \tag{2.5c}$$

Fields with such a dependence on the angle ϕ are axially symmetric. For the SU(2) gauge field a rotation around the z axis (generated by $J^3=L^3+S^3$) can be compensated by a suitable isospin transformation (generated by I^3); for the Higgs field the compensating transformation consists of isospin (I^3) and of the residual custodial spin (K^3) [8].

To restrict the ansatz further, we consider a discrete symmetry of the Lagrangian, charge conjugation invariance. (We use the definition $W^c_\mu=-W^T_\mu$, $\phi^c=\phi^*$, and $A^c_\mu=-A_\mu$.) We require invariance of the fields under the combined discrete symmetry transformations of charge conjugation, reflection through the xz plane (mirror symmetry), and an SU(2) transformation by -1 (an element of the center of the group). For the SU(2) gauge fields and the Higgs field, invariance under these combined discrete transformations leads to the conditions

$$w^1_1(\rho,z)=w^1_2(\rho,z)=w^2_1(\rho,z)=w^2_2(\rho,z)=w^3_3(\rho,z)=0 , \tag{2.6c}$$

and

$$h_3(\rho,z)=0 . \tag{2.6b}$$

These conditions actually generate the Manton ansatz [13]. For the U(1) gauge field, invariance under the combined discrete transformations leads to

$$a_1(\rho,z)=a_2(\rho,z)=0 . \tag{2.6c}$$

B. Axially symmetric energy density

The resulting energy functional E is axially symmetric

$$E=\tfrac{1}{2}\int(E_w+E_a+v^2E_h)d\phi\,\rho d\rho\,dz \tag{2.7a}$$

and has the contributions

$$\begin{aligned}E_w=&\left[\partial_\rho w^1_3+\frac{1}{\rho}(w^3_1+w^1_3)-gw^3_1w^2_3\right]^2\\ &+\left[\partial_z w^1_3+\frac{1}{\rho}w^3_2-gw^3_2w^2_3\right]^2\\ &+\left[\partial_\rho w^2_3+\frac{1}{\rho}w^2_3+gw^3_1w^1_3\right]^2\\ &+(\partial_z w^2_3+gw^3_2w^1_3)^2+(\partial_\rho w^3_2-\partial_z w^3_1)^2 ,\end{aligned} \tag{2.7b}$$

$$E_a=\left[\partial_\rho a_3+\frac{1}{\rho}a_3\right]^2+(\partial_z a_3)^2 , \tag{2.7c}$$

$$\begin{aligned}E_h=&\left[\partial_\rho h_1-\frac{g}{2}w^3_1h_2\right]^2+\left[\partial_z h_1-\frac{g}{2}w^3_2h_2\right]^2\\ &+\left[\partial_\rho h_2+\frac{g}{2}w^3_1h_1\right]^2+\left[\partial_z h_2+\frac{g}{2}w^3_2h_1\right]^2\\ &+\left[\frac{1}{\rho}h_1+\frac{g}{2}(w^1_3h_2-w^2_3h_1)-\frac{g'}{2}a_3h_1\right]^2\\ &+\left[\frac{g}{2}(w^1_3h_1+w^2_3h_2)-\frac{g'}{2}a_3h_2\right]^2\\ &+\frac{\lambda v^2}{2}(h^2_1+h^2_2-1)^2 .\end{aligned} \tag{2.7d}$$

C. Residual U(1) gauge invariance

The energy functional Eq. (2.7) is still invariant under gauge transformations generated by

$$U=e^{i\Gamma(\rho,z)\tau^i u^i_3} , \tag{2.8}$$

again analogous to the energy density of multimonopoles [13,16]. Under such a gauge transformation the two-

dimensional (2D) Higgs doublets (h_1,h_2) and $(w_3^1,w_3^2-1/g\rho)$ transform with angle $\Gamma(\rho,z)$ and $2\Gamma(\rho,z)$, respectively, while the 2D gauge field (w_1^3,w_2^3) transforms inhomogeneously.

In order to construct the sphaleron solution, we have to fix a gauge.

1. "Coulomb gauge"

We will present most of our results for the sphaleron in the following gauge, which we will refer to as the "Coulomb gauge." We fix the gauge degree of freedom by choosing the gauge condition

$$G_{\rm GF}=\partial_\rho w_1^3+\partial_z w_2^3=0 \ . \tag{2.9}$$

This gauge is implemented by adding the term

$$\frac{\xi}{2}\int (G_{\rm GF})^2 d\phi\,\rho d\rho\,dz \tag{2.10}$$

to the energy functional with $\xi=1$.

2. "Hedgehog gauge"

In the "hedgehog gauge," the Higgs field assumes the "hedgehog" form

$$\phi'(\mathbf{r})=U_h\Phi(\mathbf{r})=i\tau^i\hat{\mathbf{r}}^i L(\rho,z)\frac{v}{\sqrt{2}}\begin{bmatrix}0\\1\end{bmatrix}, \tag{2.11}$$

where $\hat{\mathbf{r}}$ denotes the unit vector. In this gauge the Higgs field is described by only one unknown function $L(\rho,z)$. Starting from a regular sphaleron solution with the Higgs field

$$\Phi(\mathbf{r})=i[\tau^i u_1^i h_1(\rho,z)+\tau^i u_2^i h_2(\rho,z)]\frac{v}{\sqrt{2}}\begin{bmatrix}0\\1\end{bmatrix}$$

the gauge transformation U_h to the "hedgehog gauge" involves the function $\Gamma_h(\rho,z)$, determined via

$$\tan\Gamma_h(\rho,z)=\frac{-zh_1(\rho,z)+\rho h_2(\rho,z)}{\rho h_1(\rho,z)+zh_2(\rho,z)} \tag{2.12}$$

3. "Physical gauge"

We also consider the "physical gauge," where the Higgs field assumes its vacuum expectation value asymptotically. In this gauge the Higgs field assumes the form

$$\Phi'(\mathbf{r})=L(\rho,z)\frac{v}{\sqrt{2}}\begin{bmatrix}0\\1\end{bmatrix} . \tag{2.13}$$

It is obtained from the "hedgehog gauge" by the further transformation

$$U_p=e^{i(\pi/2)\tau^i\hat{r}^i}=i\tau^i\hat{r}^i \ . \tag{2.14}$$

While E_w remains form invariant under this transformation, E_h changes to

$$\begin{aligned}E_h=&(\partial_\rho L)^2+(\partial_z L)^2\\&+L^2\left[\frac{g}{2}\right]^2[(w'^3_1)^2+(w'^3_2)^2+(w'^1_3)^2]\\&+L^2\left[\frac{g}{2}w'^2_3-\frac{g'}{2}a_3\right]^2+\frac{\lambda v^2}{2}(L^2-1)^2 \ .\end{aligned} \tag{2.15}$$

D. Ansatz with parity reflection symmetry

In addition to the axial and mirror symmetries imposed above, we now also require parity reflection symmetry. Changing to spherical coordinates, we define the functions $F_i(r,\theta)$:

$$\begin{aligned}w_1^3(r,\theta)&=\frac{2}{gr}F_1(r,\theta)\cos\theta \ ,\\ w_2^3(r,\theta)&=-\frac{2}{gr}F_2(r,\theta)\sin\theta \ ,\\ w_3^1(r,\theta)&=-\frac{2}{gr}F_3(r,\theta)\cos\theta \ ,\\ w_3^2(r,\theta)&=\frac{2}{gr}F_4(r,\theta)\sin\theta \ ,\end{aligned} \tag{2.16a}$$

$$h_1(r,\theta)=F_5(r,\theta)\sin\theta \ , \quad h_2(r,\theta)=F_6(r,\theta)\cos\theta \ , \tag{2.16b}$$

and

$$a_3(r,\theta)=\frac{2}{g'r}F_7(r,\theta)\sin\theta \ . \tag{2.16c}$$

Then parity invariance corresponds to

$$F_i(r,\theta)=F_i(r,\pi-\theta) \ , \quad i=1,\ldots,7 \ . \tag{2.16d}$$

With these functions $F_i(r,\theta)$ the spherically symmetric ansatz, valid in the limit $g'\to 0$, is recovered when

$$\begin{aligned}&F_1(r,\theta)=F_2(r,\theta)=F_3(r,\theta)=F_4(r,\theta)=f(r) \ ,\\ &F_5(r,\theta)=F_6(r,\theta)=h(r)\end{aligned}$$

and

$$F_7(r,\theta)=0 \ ,$$

where the functions $f(r)$ and $h(r)$ correspond to those of Ref. [6].

E. Boundary conditions

1. "Coulomb gauge"

To obtain regular, finite energy solutions with the imposed symmetries, we choose as boundary conditions for the functions $F_i(r,\theta)$ in the "Coulomb gauge" [12]:

$$\begin{aligned}&r=0: \ F_i(r,\theta)|_{r=0}=0, \quad i=1,\ldots,7 \ ,\\ &r\to\infty: \ F_i(r,\theta)|_{r=\infty}=1 \ , \quad i=1,\ldots,6, \quad F_7(r,\theta)|_{r=\infty}=0 \ ,\\ &\theta=0: \ \partial_\theta F_i(r,\theta)|_{\theta=0}=0 \ , \quad i=1,\ldots,7 \ ,\\ &\theta=\pi/2: \ \partial_\theta F_i(r,\theta)|_{\theta=\pi/2}=0 \ , \quad i=1,\ldots,7 \ .\end{aligned} \tag{2.17}$$

In the "Coulomb gauge" we must then solve for all seven functions $F_i(r,\theta)$. Inspection of the energy density Eq. (2.7d) yields for the long-ranged functions $F_3(r,\theta)$, $F_4(r,\theta)$, and $F_7(r,\theta)$ the asymptotic relations

$$\begin{aligned} &F_3(r,\theta)\to 1-2\sin^2\theta F_7(r,\theta)\ , \\ &F_4(r,\theta)\to 1-(2\sin^2\theta-1)F_7(r,\theta)\ . \end{aligned} \tag{2.18}$$

2. *"Hedgehog gauge"*

In the "hedgehog gauge" there are only six independent functions, since

$$F_5(r,\theta)=F_6(r,\theta)=L(r,\theta)\ . \tag{2.19}$$

Taking Eq. (2.19) into account, the boundary conditions are the same as in Eq. (2.17). The "hedgehog gauge" was used by Rebbi and Rossi [16] for the construction of multimonopoles.

3. *"Physical gauge"*

In the "physical gauge" the SU(2) gauge field functions $F_i(r,\theta), i=1,..,4$, change according to

$$\begin{aligned} &F_i(r,\theta)\to 1-F_i(r,\theta),\quad i=1,2, \\ &F_3(r,\theta)\to 1-F_3(r,\theta) \\ &\qquad +2\sin^2\theta[F_3(r,\theta)-F_4(r,\theta)]\ , \\ &F_4(r,\theta)\to 1-F_4(r,\theta) \\ &\qquad -2\cos^2\theta[F_3(r,\theta)-F_4(r,\theta)] \end{aligned} \tag{2.20}$$

with respect to the "hedgehog gauge," while the Higgs field function $L(r,\theta)$ remains unchanged. Here only the functions $F_4(r,\theta)$ and $F_7(r,\theta)$ are long ranged with the asymptotic relation

$$F_4(r,\theta)\to F_7(r,\theta)\ . \tag{2.21}$$

F. Parameters

With the appropriate boundary conditions we solve numerically for the functions $F_i(r,\theta)$, using dimensionless coordinates $x=gvr$. We fix the parameters $g=0.65$ and $M_W=80$ GeV. We vary the Higgs-boson mass, though most calculations are performed for $M_H=M_W$; and we vary the mixing angle between $0\le\theta_W\le\pi/2$, with physical value $\theta_W=0.5$.

III. RESULTS: LEGENDRE POLYNOMIAL EXPANSION

To construct the sphaleron at finite mixing angle θ_w in general we have to solve a system of coupled nonlinear *partial* differential equations. Since this is a demanding numerical task, we will first discuss an approximate method of solution: We expand the functions $F_i(x,\theta)$, depending on two variables, in terms of Legendre polynomials $P_l(\cos\theta)$. By minimizing the energy functional we then obtain a system of coupled nonlinear *ordinary* differential equations for the unknown coefficient functions $f_{i,l}(x)$, which is solved numerically.

Such an expansion in terms of Legendre polynomials was applied by Rebbi and Rossi [16] for the construction of multimonopoles. But instead of solving differential equations for the functions $f_{i,l}(x)$, they introduced an additional expansion for the functions $f_{i,l}(x)$ and then minimized the energy functional with respect to the resulting sets of constant coefficients.

Because of the parity reflection symmetry of the sphaleron only even Legendre polynomials contribute in the expansion [16], i.e., $l=0,2,4,6\ldots$. In the following we will first discuss the zeroth-order expansion, and then the higher-order expansions, presenting results up to the sixth order.

A. Zeroth-order Legendre polynomial expansion

In the limit of vanishing mixing angle, the sphaleron is spherical. Therefore an expansion in Legendre polynomials would have only nonvanishing lowest-order terms

$$F_i(x,\theta)=f_{i,0}(x)P_0(\cos\theta)=f_{i,0}(x)\ . \tag{3.1}$$

For small but finite mixing angles, one expects that the zeroth-order expansion will do quite well, while for larger mixing angles higher-order terms should become increasingly important.

Requiring a finite energy density and a finite energy leads to a restriction on the zeroth-order functions $f_{i,0}(x)$. The SU(2) gauge part of the energy density Eq. (2.7b) contains in its first term the expression

$$\frac{1}{\rho}(w_1^3+w_3^1)=\frac{2gv^2}{x^2}[F_1(x,\theta)-F_3(x,\theta)]\frac{\cos\theta}{\sin\theta}\ , \tag{3.2a}$$

which implies a singular behavior along the z axis unless

$$F_1(x,\theta=0)=F_3(x,\theta=0)\ . \tag{3.2b}$$

Since the zeroth order the functions $F_i(x,\theta)$ do not depend on θ, we must require

$$f_{1,0}(x)=f_{3,0}(x) \tag{3.2c}$$

to avoid the singular behavior. This leaves one independent function $f_{i,0}(x)$ less to be determined.

In the following we consider the zeroth-order expansion in the "Coulomb gauge" and in the "physical gauge," and the further restricted expansion of Ref. [17].

1. *"Coulomb gauge"*

Because of the restriction (3.2c) in the "Coulomb gauge" six independent functions $f_{i,0}(x)$ ought be determined. Inspection of the asymptotic relations (2.18), however, shows that this gauge is inadequate when only zeroth-order terms are taken into account. These relations clearly require an asymptotic θ dependence for the functions $F_3(x,\theta)$ and $F_4(x,\theta)$, if $F_7(x,\theta)$ is long ranged, even if $F_7(x,\theta)$ were independent of θ. Thus not allowing for a θ dependence of all three functions would imply that none of these functions could be long ranged. This would physically not be acceptable, since also the mass-

less photon is described by a combination of these functions. Thus the "Coulomb gauge" is inadequate in zeroth order.

2. *"Physical gauge"*

A better gauge for the zeroth-order approximation is the "physical gauge." Here the asymptotic condition (2.21) allows both functions $F_4(x,\theta)$ and $F_7(x,\theta)$ to be long ranged, thus yielding the proper asymptotic behavior for the electromagnetic field. Since in this gauge we have the condition

$$f_{5,0}(x)=f_{6,0}(x) \tag{3.3}$$

in addition to condition (3.2c), there remain only five independent functions $f_{i,0}(x)$ to be determined.

The energy of the sphaleron in the zeroth order in the "physical gauge" is shown as a function of the mixing angle in Fig. 1(a) for $M_H=M_W$. In the zeroth order the energy density is finite in this gauge. In the limit $\theta_w=\pi/2$, the variational principle yields the relation

$$f_{7,0}(x)=f_{4,0}(x) .$$

3. *Restricted calculation of Ref. [17]*

The results of Klinkhamer and Laterveer [17] are obtained, when in the "physical gauge" the functions $f_{i,0}(x)$ are further restricted according to

$$f_{1,0}(x)=f_{2,0}(x)=f_{3,0}(x) . \tag{3.4}$$

This leaves only four functions to be determined. For comparison, we also show these results in Fig. 1(a) for $M_H=M_W$.

B. Higher-order Legendre polynomial expansion

We turn now to the general expansion in terms of Legendre polynomials. Following Rebbi and Rossi [16] we expand the functions $F_i(x,\theta)$ as follows:

$$F_1(x,\theta)=f_{1,0}(x)+\sum_{l=2}^{2N} f_{1,l}(x)\frac{\cos^2\theta-1}{l\cos\theta}\frac{dP_l(\cos\theta)}{d\cos\theta} , \tag{3.5a}$$

$$F_2(x,\theta)=f_{2,0}(x)+\sum_{l=2}^{2N} f_{2,l}(x)\frac{\cos\theta}{l}\frac{dP_l(\cos\theta)}{d\cos\theta} , \tag{3.5b}$$

$$F_3(x,\theta)=f_{1,0}(x)+\sum_{l=2}^{2N} f_{3,l}(x)\frac{\cos^2\theta-1}{l\cos\theta}\frac{dP_l(\cos\theta)}{d\cos\theta} , \tag{3.5c}$$

$$F_4(x,\theta)=f_{4,0}(x)+\sum_{l=2}^{2N} f_{4,l}(x)\frac{\cos\theta}{l}\frac{dP_l(\cos\theta)}{d\cos\theta} , \tag{3.5d}$$

$$F_5(x,\theta)=f_{5,0}(x)+\sum_{l=2}^{2N} f_{5,l}(x)P_l(\cos\theta) , \tag{3.5e}$$

$$F_6(x,\theta)=f_{6,0}(x)+\sum_{l=2}^{2N} f_{6,l}(x)P_l(\cos\theta) , \tag{3.5f}$$

$$F_7(x,\theta)=f_{7,0}(x)+\sum_{l=2}^{2N} f_{7,l}(x)P_l(\cos\theta) , \tag{3.5g}$$

where l assumes only even values due to the parity reflection symmetry. The higher-order terms in the ex-

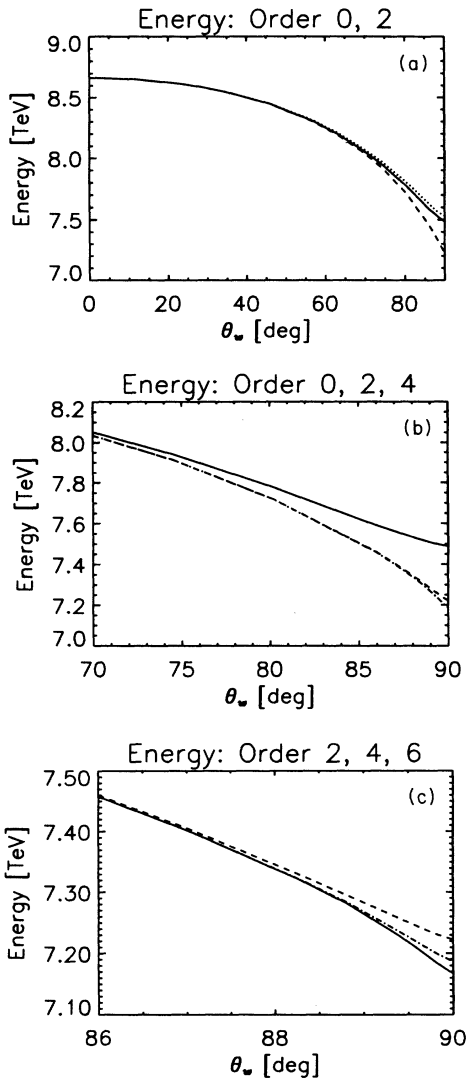

FIG. 1. The energy of the sphaleron (in units of TeV) is shown as a function of the mixing angle θ_W for $M_H=M_W$. (a) The solid curve represents the zeroth-order calculation ("physical gauge"), the dashed curve represents the second-order calculation ("Coulomb gauge"), and the dotted curve represents the approximation of Ref. [17]. (b) The solid curve represents the zeroth-order calculation ("physical gauge"), the dashed curve represents the second-order calculation ("Coulomb gauge"), and the dot-dashed curve represents the fourth-order calculation ("Coulomb gauge"). (c) The dashed curve represents the second-order calculation ("Coulomb gauge"), the dot-dashed curve represents the fourth-order calculation ("Coulomb gauge"), and the solid curve represents the sixth-order calculation ("physical gauge").

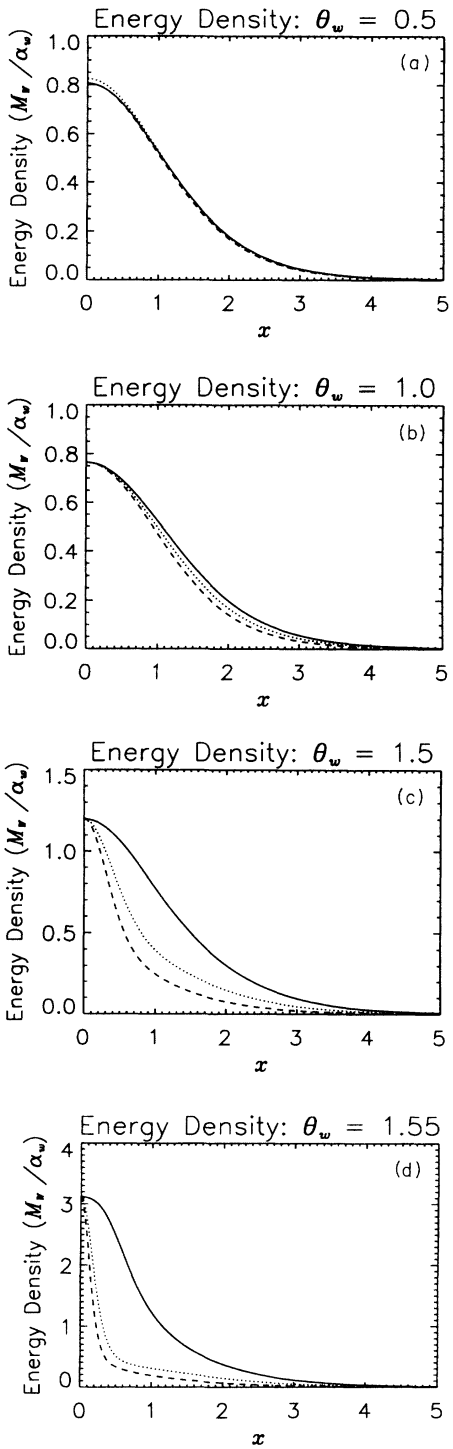

FIG. 2. The energy density of the sphaleron (in units of M_W/α_w) obtained in the sixth-order calculation ("Coulomb gauge") is shown as a function of the dimensionless coordinate x at $\theta_w=0.5$ for $M_H=M_W$. (a) The solid and the dashed curves represent the angles $\theta=0$ and $\theta=\pi/2$, respectively. For comparison, the dotted curve represents the energy density of the spherical sphaleron at $\theta_w=0$. (b) For $\theta_w=1.0$; solid curve: angle $\theta=0$, dotted curve: angle $\theta=\pi/4$, dashed curve: angle $\theta=\pi/2$. (c) For $\theta_w=1.5$; solid curve: angle $\theta=0$, dotted curve: angle $\theta=\pi/4$, dashed curve: angle $\theta=\pi/2$. (d) For $\theta_w=1.55$; solid curve: angle $\theta=0$, dotted curve: angle $\theta=\pi/4$.

pansion of $F_1(x,\theta)$ and $F_3(x,\theta)$ are proportional to $\sin^2\theta$, while for $F_2(x,\theta)$ and $F_4(x,\theta)$ they are proportional to $\cos^2\theta$. The constraint (3.2b) requires the condition (3.2c) for the zeroth-order functions in the expansion of $F_1(x,\theta)$ and $F_3(x,\theta)$, but the $\sin^2\theta$ dependence of the higher-order terms in the expansion makes these contributions regular without the need for further constraining conditions.

We will put our main emphasis on the calculations in the "Coulomb gauge," since these results will be directly compared with the corresponding results from the integration of the *partial* differential equations in Sec. IV.

1. *"Coulomb gauge"*

In contrast with the zeroth-order expansion, for the higher-order expansions the "Coulomb gauge" is an adequate choice of gauge, since the asymptotic relations (2.18) can now be satisfied with long-ranged fields. We have performed calculations in the "Coulomb gauge" for expansions of second, fourth, and sixth order. This involves solving systems of $(6+7l/2)$ coupled *ordinary* differential equations. Obviously, the computational effort increases significantly with each order.

Let us first discuss the gauge-invariant quantities, the energy, the energy density and the magnetic moment, as functions of the mixing angle θ_w. Figure 1 shows the energy of the electroweak sphaleron obtained in zero order in the "physical gauge," and in second, fourth, and sixth order in the "Coulomb gauge" for $M_H=M_W$. The energy decreases as a function of the mixing angle, for small θ_w only slightly, for larger θ_w stronger. The higher-order terms affect the energy only at larger values of the mixing angle. Each higher order lowers the energy only beyond increasingly larger values of θ_w. But in each order the energy reaches a finite lower limiting value for $\theta_w=\pi/2$.

Let us now consider the convergence of the expansion as illustrated in Fig. 1. In Fig. 1(a) we compare the energies from the second-order calculation in the "Coulomb gauge" with the corresponding energies from the zeroth-order calculations in the "physical gauge." We observe that up to quite large values of the mixing angle the

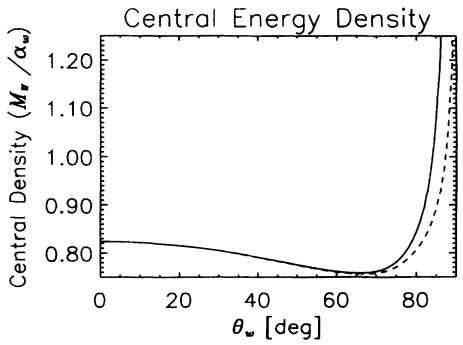

FIG. 3. The energy density of the sphaleron at the origin (in units of M_W/α_w) is shown as a function of the mixing angle θ_w for $M_H=M_W$. The dashed curve represents the zeroth-order calculation ("physical gauge"), and the solid curve represents the sixth-order calculation ("Coulomb gauge").

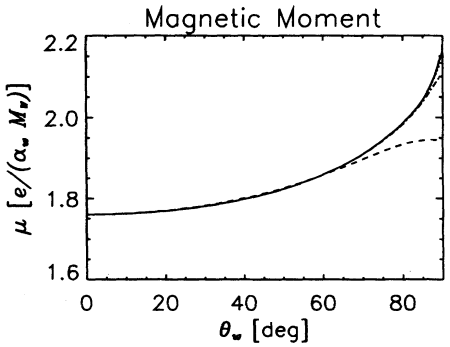

FIG. 4. The magnetic dipole moment of the sphaleron (in units of $e/\alpha_w M_W$) is shown as a function of the mixing angle θ_w for $M_H = M_W$. The dashed curve represents the zeroth-order calculation ("physical gauge"), the dot-dashed curve represents the second-order calculation ("Coulomb gauge"), the dotted curve represents the fourth-order calculation ("Coulomb gauge"), and the solid curve represents the sixth-order calculation ("Coulomb gauge").

zeroth-order approximation is remarkably good. At $\theta_w = 0.5$, the physical value of the mixing angle, the zeroth-order approximation yields an energy value only 0.001% higher than the second-order approximation, and the discrepancy increases only slowly. It is 0.01% at $\theta_w = 0.8$, 0.1% at $\theta_w = 1.1$, and reaches 3.7% in the limit $\theta_w = \pi/2$. The fourth-order results are shown in Fig. 1(b). The energies of the fourth-order expansion begin to deviate from those of the second-order expansion only at $\theta_w = 1.2$, where the difference is 0.001%. The sixth-order results finally deviate from the fourth-order results only beyond $\theta_w = 1.5$, reaching 0.001% at $\theta_w = 1.52$. They are illustrated in Fig. 1(c) for large θ_w.

Let us now consider the energy density. In Figs. 2(a)–2(d) we illustrate the energy density as a function of the spatial coordinates x and θ, for the mixing angles $\theta_w = 0.5$, 1.0, 1.5, and 1.55, and for $M_H = M_W$. At the physical mixing angle $\theta_w = 0.5$ the energy density is hardly deformed and differs only little from the spherical energy density. Then with increasing mixing angle θ_w the sphaleron becomes more and more deformed. The energy density is larger along the z axis (for angle $\theta = 0$) and smaller along the ρ axis (for angle $\theta = \pi/2$). Equal density contours form ellipsoids, which become increasingly elongated in the z direction for increasingly large values of the mixing angle.

The energy density at the origin, the central density, is shown as a function of the mixing angle in Fig. 3 for $M_H = M_W$ for the zeroth-order calculation in the "physi-

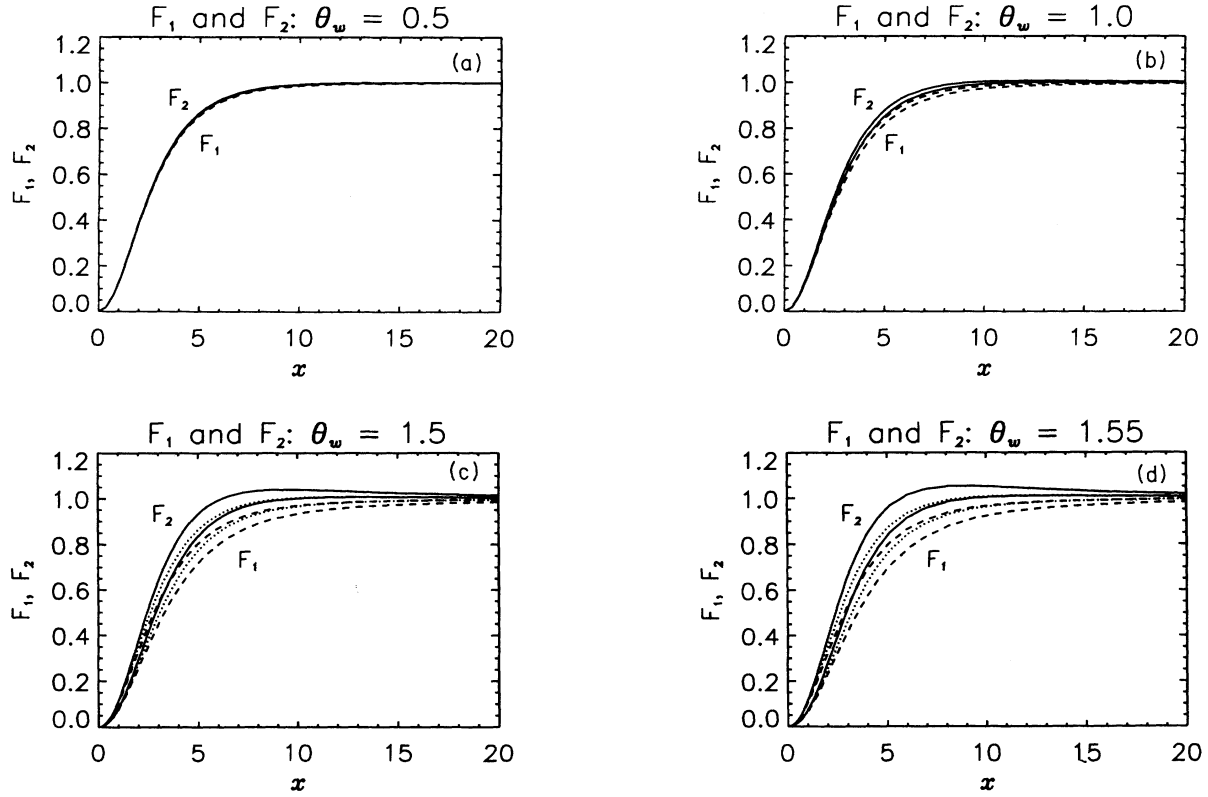

FIG. 5. The SU(2) gauge field functions $F_1(x,\theta)$ and $F_2(x,\theta)$ obtained in the sixth-order calculation ("Coulomb gauge") are shown as a function of the dimensionless coordinate x at $\theta_w = 0.5$ for $M_H = M_W$. (a) The solid and the dashed curves represent the angles $\theta = 0$ and $\theta = \pi/2$, respectively. The curves for $F_1(x,\theta)$ are slightly below those for $F_2(x,\theta)$. (See the larger mixing angles.) (b) For $\theta_w = 1.0$; solid curves: angle $\theta = 0$, dashed curves: angle $\theta = \pi/2$. (c) For $\theta_w = 1.5$; solid curves: angle $\theta = 0$, dotted curves: angle $\theta = \pi/4$, dashed curves: angle $\theta = \pi/2$. (d) For $\theta_w = 1.55$; solid curves: angle $\theta = 0$, dotted curves: angle $\theta = \pi/4$, dashed curves: angle $\theta = \pi/2$.

cal gauge" and for the sixth-order calculation in the "Coulomb gauge." With increasing mixing angle the central density decreases first slightly. Then it reaches a minimum at $\theta_w \approx 1.2$. When the mixing angle approaches the value $\theta_w = \pi/2$, the central density (in the "Coulomb gauge") diverges rapidly. The higher the order of the calculation the earlier the dramatic increase of the central density sets in.

Another interesting physical quantity characterizing the electroweak sphaleron is its magnetic dipole moment μ. The electromagnetic field of the electroweak sphaleron has the asymptotic behavior

$$\mathbf{A}_{\mathrm{EM}}(\mathbf{r}) \rightarrow \frac{\boldsymbol{\mu} \times \mathbf{r}}{4\pi r^3} , \tag{3.6a}$$

where $\mathbf{u}=(0,0,\mu)$ represents the magnetic dipole moment. It can be extracted from the long-range behavior of the functions $F_3(x,\theta)$, $F_4(x,\theta)$, and $F_7(x,\theta)$. To extract this magnetic dipole moment we perform an (asymptotic) gauge transformation, which changes the asymptotically twisted Higgs field in the "Coulomb gauge" to the "physical gauge." Applying this transformation to the SU(2) gauge field yields the "physical" asymptotic isospin-3 component of the gauge field, needed to construct the asymptotic behavior of the electromagnetic field and of the massive Z^0 field. The magnetic dipole moment is then obtained as

$$\mu = \frac{e}{\alpha_w M_W} \Xi , \quad \Xi = x F_7(x) \frac{g^2}{e^2} \quad (x \rightarrow \infty) . \tag{3.6b}$$

The magnetic dipole moment as a function of the mixing angle is shown in Fig. 4 for $M_H = M_W$ for the zeroth-order calculation in the "physical gauge" and for the second- fourth-, and sixth-order calculations in the "Coulomb gauge." The convergence properties of the expansion as a function of the mixing angle θ_w are for the magnetic dipole moment similar to those for the energy discussed above. At the physical value of the mixing angle we find a magnetic dipole moment which is only slightly different from the value obtained by Klinkhamer and Manton [6] applying perturbation theory. Thus we confirm their remarkable result that the electroweak sphaleron has a very big magnetic dipole moment.

We finally turn to the functions $F_i(x,\theta)$ themselves, which are gauge dependent except for the U(1) field function $F_7(x,\theta)$ and the length function of the Higgs field $L(x,\theta)$:

$$L(x,\theta) = \sqrt{F_5(x,\theta)^2 \sin^2\theta + F_6(x,\theta)^2 \cos^2\theta} .$$

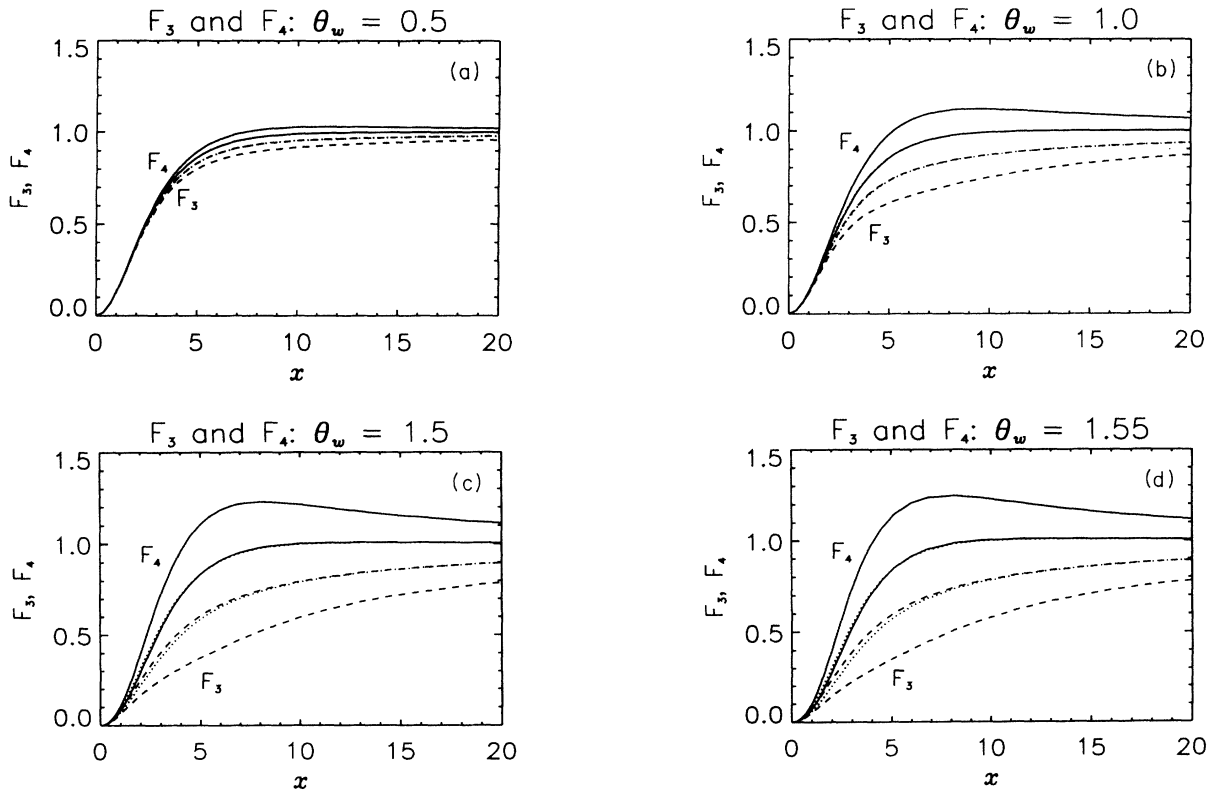

FIG. 6. The SU(2) gauge field functions $F_3(x,\theta)$ and $F_4(x,\theta)$ obtained in the sixth-order calculation ("Coulomb gauge") are shown as a function of the dimensionless coordinate x at $\theta_w = 0.5$ for $M_H = M_W$. (a) The solid, the dotted, and the dashed curves represent the angles $\theta=0$, $\theta=\pi/4$, and $\theta=\pi/2$, respectively. (See the larger mixing angles.) (b) For $\theta_w = 1.0$; solid curves: angle $\theta=0$, dotted curves: angle $\theta=\pi/4$, dashed curves: angle $\theta=\pi/2$. (c) For $\theta_w = 1.5$; solid curves: angle $\theta=0$, dotted curves: angle $\theta=\pi/4$, dashed curves: angle $\theta=\pi/2$. (d) For $\theta_w = 1.55$; solid curves: angle $\theta=0$, dotted curves: angle $\theta=\pi/4$, dashed curves: angle $\theta=\pi/2$.

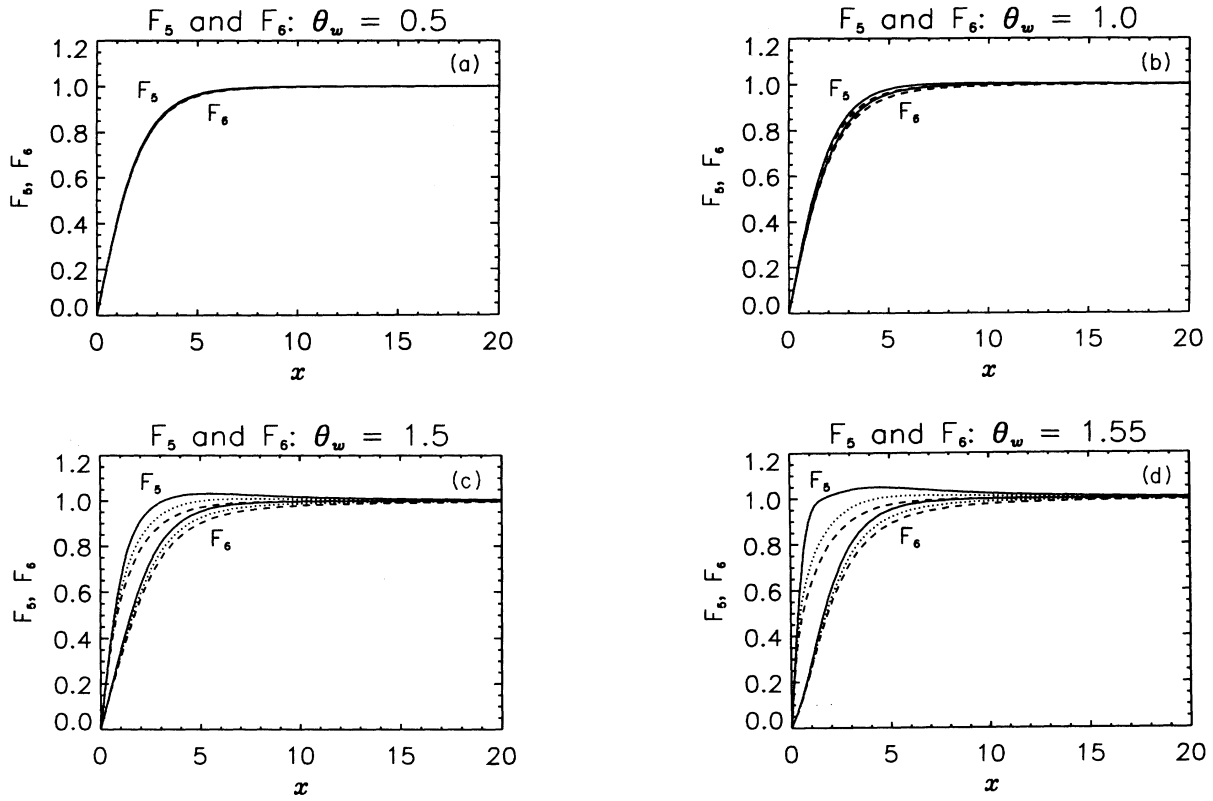

FIG. 7. The Higgs field functions $F_5(x,\theta)$ and $F_6(x,\theta)$ obtained in the sixth-order calculation ("Coulomb gauge") are shown as a function of the dimensionless coordinate x at $\theta_w=0.5$ for $M_H=M_W$. (a) The solid and the dashed curves represent the angles $\theta=0$ and $\theta=\pi/2$, respectively. The curves for $F_5(x,\theta)$ are slightly above those for $F_6(x,\theta)$. (See the larger mixing angles.) (b) For $\theta_w=1.0$; solid curves: angle $\theta=0$, dashed curves: angle $\theta=\pi/2$. (c) For $\theta_w=1.5$; solid curves: angle $\theta=0$, dotted curves: angle $\theta=\pi/4$, dashed curves: angle $\theta=\pi/2$. (d) For $\theta_w=1.55$; solid curves: angle $\theta=0$, dotted curves: angle $\theta=\pi/4$, dashed curves: angle $\theta=\pi/2$.

Figures 5–8 show the functions $F_1(x,\theta)$ and $F_2(x,\theta)$, $F_3(x,\theta)$ and $F_4(x,\theta)$, $F_5(x,\theta)$ and $F_6(x,\theta)$, $F_7(x,\theta)$ and $L(x,\theta)$, obtained with calculations of the sixth order, for the mixing angles $\theta_w=0.5$, 1.0, 1.5, and 1.55 and for $M_H=M_W$. The figures clearly demonstrate the effect which an increase of the mixing angle has on the functions.

At $\theta_w=0.5$ there is hardly any angular θ dependence noticeable in the functions $F_i(x,\theta)$, except for the trivial asymptotic θ dependence of $F_3(x,\theta)$ and $F_4(x,\theta)$, implied by the asymptotic relations (2.18). At $\theta_w=1.0$ a noticeable nontrivial θ dependence of the functions $F_i(x,\theta)$ in the inner region of the sphaleron has developed and keeps increasing with increasing mixing angle.

We observe that at the origin with increasing mixing angle the functions $F_1(x,\theta)$ and $F_2(x,\theta)$ tend more and more apart from each other, and likewise the functions $F_5(x,\theta)$ and $F_6(x,\theta)$. For the latter we further observe that for $\theta_w\to\pi/2$ the slope of $F_5(x,\theta)$ at the origin tends to infinity, while the slope of $F_6(x,\theta)$ tends to zero:

$$\frac{dF_5(x,\theta)}{dx}\xrightarrow[x\to 0]{}\infty\ , \tag{3.7a}$$

$$\frac{dF_6(x,\theta)}{dx}\xrightarrow[x\to 0]{}0\ . \tag{3.7b}$$

It is this behavior (3.7a) of the Higgs field which leads to the divergence of the energy density at the origin in the limit $\theta_w\to\pi/2$.

For very large values of the mixing angle the most dramatic changes appear in the functions $F_5(x,\theta)$, $F_6(x,\theta)$, and $F_7(x,\theta)$. In particular, for small angles θ the functions $F_5(x,\theta)$ and $F_7(x,\theta)$ develop pronounced peaks. This is demonstrated in Figs. 9 and 10, where for comparison we present the fourth- and the sixth-order results for the mixing angles $\theta_w=1.55$, 1.56, and 1.57.

Comparing all the results obtained in the various orders we conclude that the zeroth-order approximation in the "physical gauge" is excellent up to the physical value of the mixing angle $\theta_w=0.5$. In the "Coulomb gauge" the second-order approximation is as good and fully sufficient up to $\theta_w=1.2$ and the fourth-order approximation up to $\theta_w=1.52$. Up to which value of the mixing angle the sixth-order calculation does well, we will see in Sec. IV, where we compare with the results obtained by directly integrating the *partial* differential equations. For very large values of the mixing angle the expansion obviously has not yet converged.

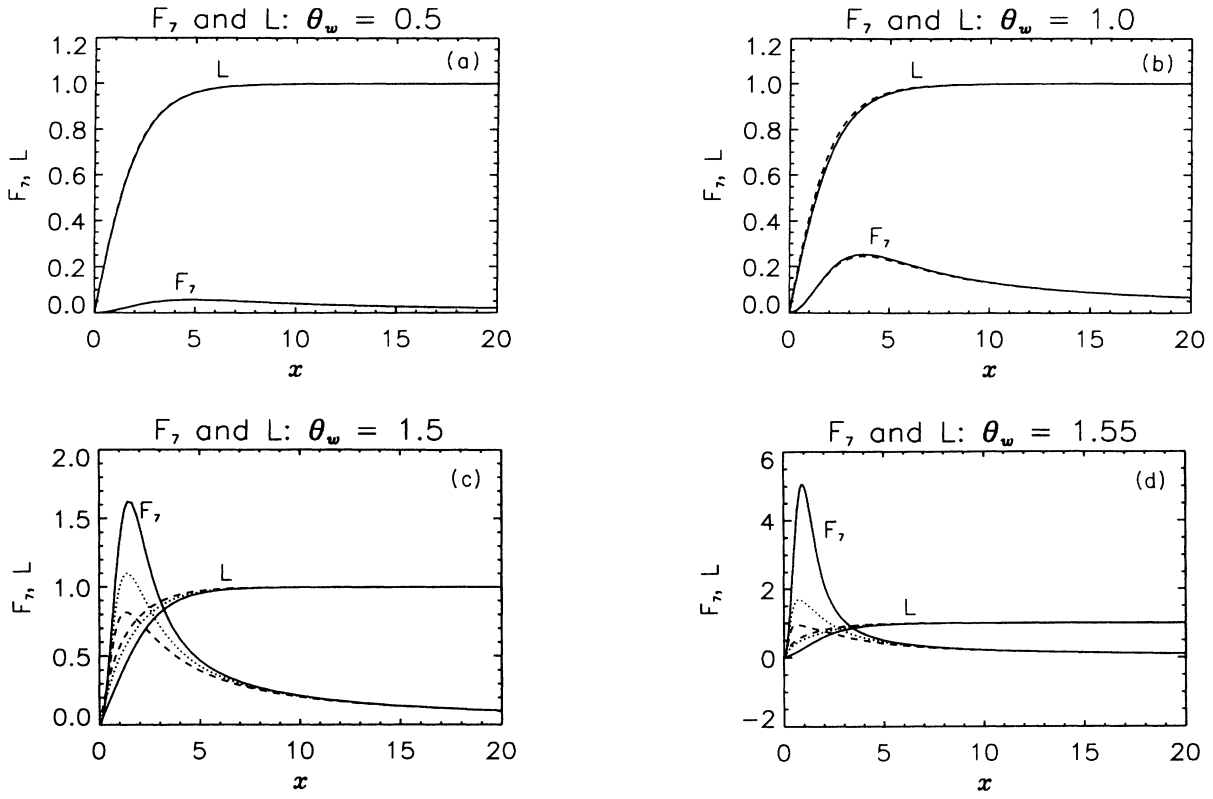

FIG. 8. The U(1) gauge field function $F_7(x,\theta)$ and the length function of the Higgs field $L(x,\theta)$ obtained in the sixth-order calculation ("Coulomb gauge") are shown as a function of the dimensionless coordinate x at $\theta_w=0.5$ for $M_H=M_W$. (a) The solid and the dashed curves represent the angles $\theta=0$ and $\theta=\pi/2$, respectively. (b) For $\theta_w=1.0$; solid curves: angle $\theta=0$, dashed curves: angle $\theta=\pi/2$. (c) For $\theta_w=1.5$; solid curves: angle $\theta=0$, dotted curves: angle $\theta=\pi/4$, dashed curves: angle $\theta=\pi/2$. (d) For $\theta_w=1.55$; solid curves: angle $\theta=0$, dotted curves: angle $\theta=\pi/4$, dashed curves: angle $\theta=\pi/2$.

2. *Gauge fixing by elimination of constraints*

To discuss the second gauge used for the higher-order expansion, let us return to Eqs. (3.5). Inserting this expansion of the functions $F_i(x,\theta)$ into the energy functional (2.7), where no gauge-fixing condition has as yet been chosen, we find that for the lth-order expansion there are only $(6+6l/2)$ independent propagating functions, accompanied by $(l/2)$ constraints which arise for combinations of the functions $f_{1,l}(x)$ and $f_{2,l}(x)$. Rewriting these functions for $l>0$ as the combinations

$$f_{1,l}(x)=\tilde{f}_{1,l}(x)+\tilde{f}_{2,l}(x)\ , \tag{3.8a}$$

$$f_{2,l}(x)=\tilde{f}_{1,l}(x)-\tilde{f}_{2,l}(x)\ , \tag{3.8b}$$

we see that the energy functional does not contain the derivatives of the functions $\tilde{f}_{1,l}(x)$. Therefore they lead only to constraint equations. Having isolated the constraints, we fix the gauge by demanding

$$\tilde{f}_{1,l}(x)=0\ . \tag{3.9}$$

This choice simplifies the set of *ordinary* differential equations considerably.

For gauge-independent quantities the results obtained in this gauge are in excellent agreement with those obtained in the "Coulomb gauge." Also the gauge-dependent functions $F_i(x,\theta)$ show in this gauge many features similar to the "Coulomb gauge." For instance, the functions $F_1(x,\theta)$ and $F_2(x,\theta)$ and also $F_5(x,\theta)$ and $F_6(x,\theta)$ split increasingly strongly at the origin with increasing mixing angle θ_w. But the angular θ dependence of the functions $F_1(x,\theta)$ and $F_2(x,\theta)$, and $F_5(x,\theta)$ and $F_6(x,\theta)$ themselves remains smaller than in the "Coulomb gauge." In particular, $F_5(x,\theta)$ does not develop the peak along the z axis for very large values of the mixing angle. As an example we present the functions $F_i(x,\theta)$ for $\theta_w=1.5$ and for $M_H=M_W$ in Fig. 11.

IV. RESULTS: PARTIAL DIFFERENTIAL EQUATIONS

We now present the results for the electroweak sphaleron obtained by integrating directly the set of coupled nonlinear *partial* differential equations numerically. The calculations cover the range of the mixing angle $0\le\theta_w<\pi/2$, and are performed in the "Coulomb gauge."

The numerical calculations are based on the Newton-Raphson method [18]. The equations are discretized on a nonequidistant grid in x and an equidistant grid in θ. For

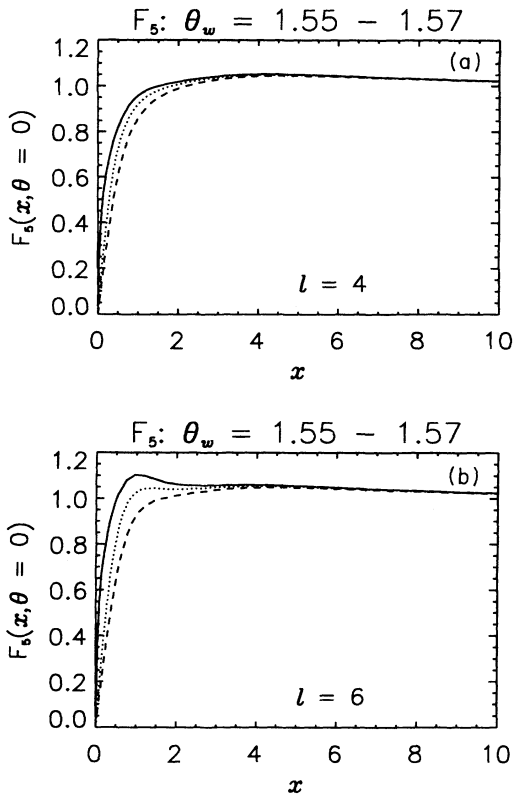

FIG. 9. The Higgs field function $F_5(x,\theta)$ obtained in the fourth-order calculation ("Coulomb gauge") is shown as a function of the dimensionless coordinate x at angle $\theta=0$ for $M_H=M_W$. (a) The dashed, dotted, and solid curves represent the mixing angles $\theta_w=1.55$, $\theta_w=1.56$, and $\theta_w=1.57$, respectively. (b) For the sixth-order calculation ("Coulomb gauge"); dashed curve: mixing angle $\theta_w=1.55$, dotted curve: mixing angle $\theta_w=1.56$, solid curve: mixing angle $\theta_w=1.57$.

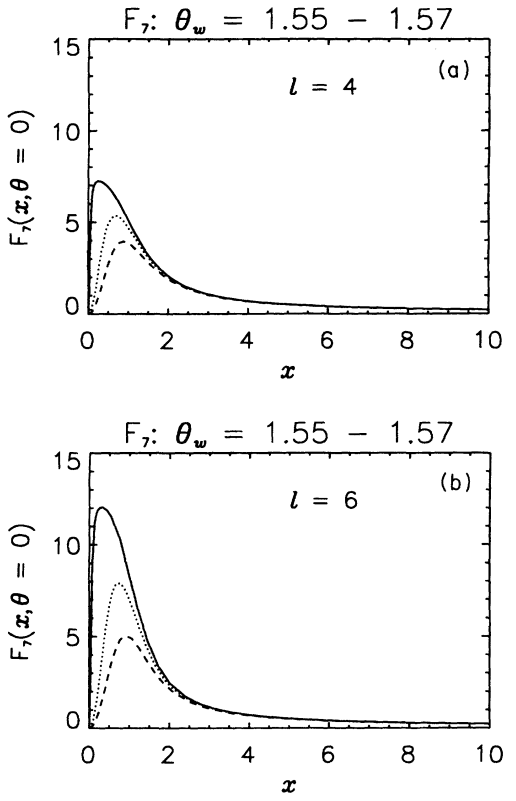

FIG. 10. The U(1) gauge field function $F_7(x,\theta)$ obtained in the fourth-order calculation ("Coulomb gauge") is shown as a function of the dimensionless coordinate x at angle $\theta=0$ for $M_H=M_W$. (a) The dashed, dotted, and solid curves represent the mixing angles $\theta_w=1.55$, $\theta_w=1.56$, and $\theta_w=1.57$, respectively. (b) For the sixth-order calculation ("Coulomb gauge"); dashed curve: mixing angle $\theta_w=1.55$, dotted curve: mixing angle $\theta_w=1.56$, solid curve: mixing angle $\theta_w=1.57$.

small mixing angles θ_w grids of sizes 50×20 and 100×20 are used, covering integrating regions $0<x<40$ and $0<x<120$, with $0<\theta<\pi/2$. For large values of θ_w the number of grid points in θ is doubled to obtain the functions $F_i(x,\theta)$ with high accuracy, i.e., a relative numerical error estimated to be smaller than 10^{-3}. However, for mixing angles very close to the limiting value $\theta_w=\pi/2$, even the larger grid size does not lead to a high numerical accuracy, and thus reliable results. In fact, for mixing angles $\theta_w>1.567$ the numerical results have a relative error on the order of 10^{-2} or even bigger for some of the functions $F_i(x,\theta)$. In particular, the error for the functions $F_5(x,\theta)$ and $F_7(x,\theta)$ along the z axis increases considerably. Our calculations are therefore much less reliable for θ_w very close to $\pi/2$. Consequently we cannot determine the limiting sphaleron configuration and its properties for $\theta_w=\pi/2$.

The numerical results for the sphaleron at finite mixing angle obtained by solving the *partial* differential equations in the "Coulomb gauge" agree (within our numerical accuracy) with the corresponding results from the highest-order Legendre polynomial expansion up to very large values of the mixing angle. This is demonstrated for the energies for $M_H=M_W$ in Fig. 12, where deviations between the sixth-order calculation and the numerical integration of the *partial* differential equations become visible only beyond $\theta_w=1.54$. Since for $\theta_w>1.567$ the numerical accuracy of the calculations becomes increasingly worse, these results are indicated by a dotted curve only. Because of the lack of accuracy we unfortunately cannot definitely decide whether the energy of the sphaleron remains finite in the limit $\theta_w\to\pi/2$, although concluding from the polynomial expansion this appears to be the case. The limiting value of the energy for $\theta_w=\pi/2$ remains thus unknown.

Also the energy densities agree with those from the polynomial expansion up to $\theta_w=1.54$. Beyond this value of the mixing angle, the energy density obtained by solving the *partial* differential equations increases stronger at the origin and thus diverges faster. The value of the energy density at the origin is shown in Fig. 13 for θ_w close to $\pi/2$ for $M_H=M_W$. Again, the less accurate results are indicated only by a dotted curve. For comparison the energy densities obtained with the zeroth-order ("physical gauge") and with the sixth-order ("Coulomb gauge") calculations are also shown. (Note the logarithmic scale.)

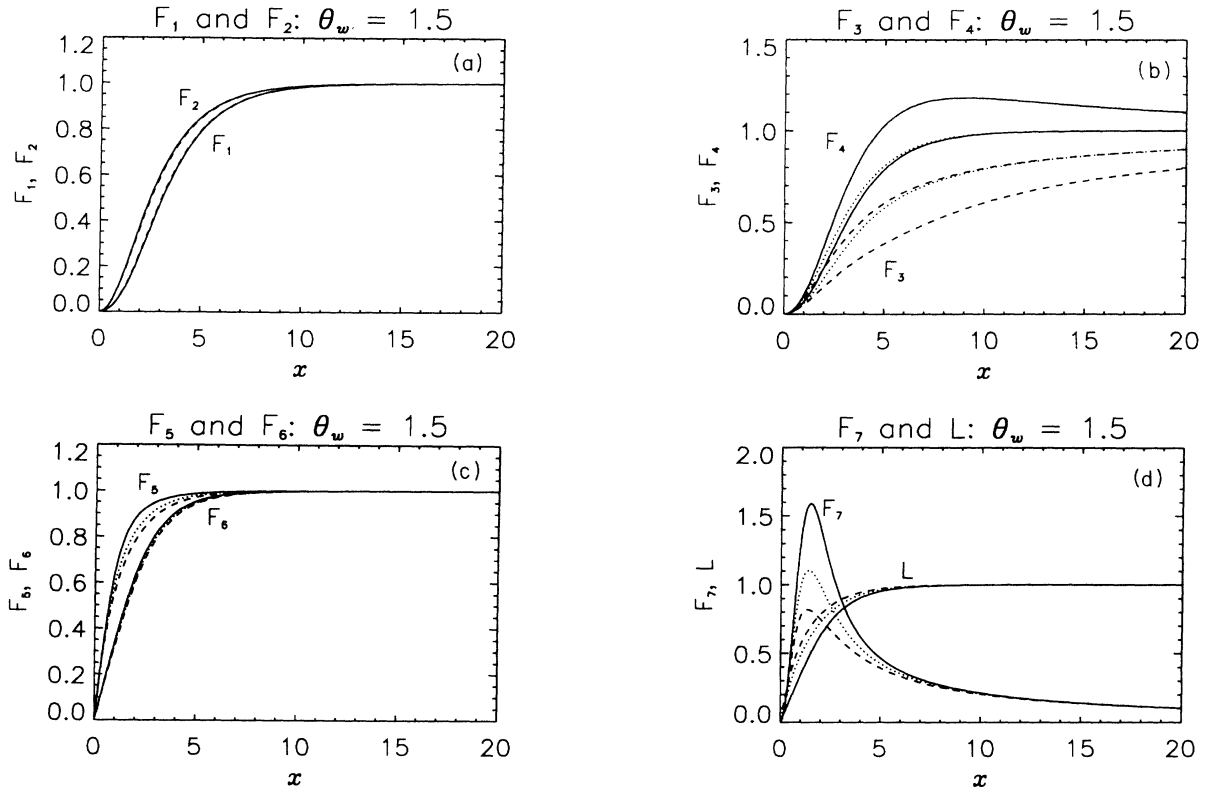

FIG. 11. The SU(2) gauge field functions $F_1(x,\theta)$ and $F_2(x,\theta)$ obtained in the fourth-order calculation with gauge fixing by eliminating the constraint functions (3.9) are shown as a function of the dimensionless coordinate x at $\theta_w=1.5$ for $M_H=M_W$. (a) The solid and the dashed curves represent the angles $\theta=0$ and $\theta=\pi/2$, respectively. (b) For the SU(2) gauge field functions $F_3(x,\theta)$ and $F_4(x,\theta)$; solid curves: angle $\theta=0$, dotted curves: angle $\theta=\pi/4$, dashed curves: angle $\theta=\pi/2$. (c) For the Higgs field functions $F_5(x,\theta)$ and $F_6(x,\theta)$; solid curves: angle $\theta=0$, dotted curves: angle $\theta=\pi/4$, dashed curves: angle $\theta=\pi/2$. For the U(1) gauge field function $F_7(x,\theta)$ and the length function of the Higgs field $L(x,\theta)$; solid curves: angle $\theta=0$, dotted curves: angle $\theta=\pi/4$, dashed curves: angle $\theta=\pi/2$.

For the functions $F_i(x,\theta)$ deviations between the sixth-order calculation ("Coulomb gauge") and the numerical integration of the *partial* differential equations begin to appear beyond $\theta_w=1.54$ as well. Again, the deviations are most apparent for the functions $F_5(x,\theta)$ and $F_7(x,\theta)$ along the z axis. The peaks in these functions develop earlier and more rapidly at large values of the mixing angle, as compared to the sixth-order polynomial calculations. This is demonstrated with the help of Fig. 14, where these functions obtained by solving the *partial* differential equations are shown. The functions of Fig. 14 should be compared with those of Figs. 9 and 10.

Thus we conclude that for $\theta_w \geq 1.54$ higher than sixth-order terms in the polynomial expansion are necessary for an accurate description of the sphaleron. The construction of the sphaleron in the limit $\theta_w=\pi/2$ remains a numerically challenging task.

V. CONCLUSIONS

We have constructed the classical sphaleron solution of the Weinberg-Salam theory for finite values of the mixing angle, $0 \leq \theta_w \leq \pi/2$. For the numerical calculations we have applied two alternative methods.

(1) We have converted the system of coupled nonlinear *partial* differential equations by means of a Legendre polynomial expansion into a system of *ordinary* differential equations and solved this system with zeroth-order up to sixth-order polynomials included.

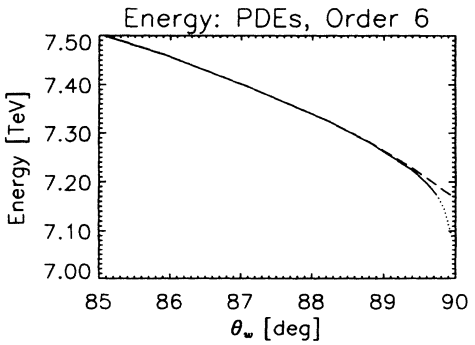

FIG. 12. The energy of the sphaleron (in units of TeV) is shown as a function of the mixing angle θ_w for $M_H=M_W$. The solid curve represents the results with high accuracy and the dotted curve those with less accuracy, obtained by integrating the partial differential equations ("Coulomb gauge"). The long-dashed curve represents the sixth-order calculation ("Coulomb gauge").

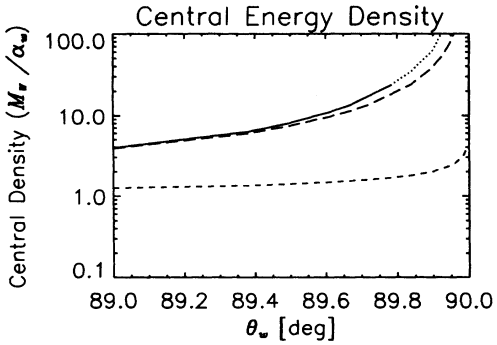

FIG. 13. The energy density of the sphaleron at the origin (in units of M_W/α_w) is shown as a function of the mixing angle θ_w for $M_H=M_W$. The solid curve represents the results with high accuracy and the dotted curve those with less accuracy, obtained by integrating the partial differential equations ("Coulomb gauge"). The long-dashed curve represents the sixth-order calculation ("Coulomb gauge"), and the short-dashed curve the zeroth-order calculation ("physical gauge").

(2) We have solved the system of coupled nonlinear *partial* differential equations directly.

Comparing the results obtained by the two methods we have found that the zeroth-order expansion in the "physical gauge" is very good for small mixing angles, even up to the physical value of the mixing angle, $\theta_w=0.5$. Choosing the "Coulomb gauge" beyond the second-order expansion is sufficient up to $\theta_w \leq 1.2$, beyond the fourth order up to $\theta_w \leq 1.52$, and beyond the sixth order for $\theta_w \leq 1.54$. Then eighth- and higher-order terms must be included.

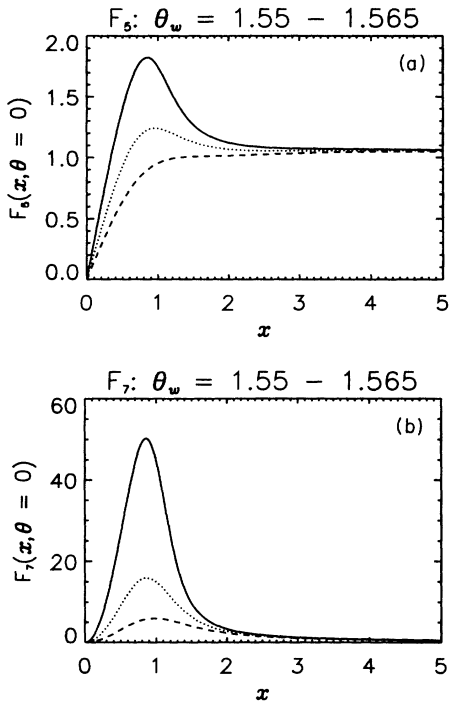

FIG. 14. The Higgs field function $F_5(x,\theta)$ obtained by integrating the partial differential equations ("Coulomb gauge") is shown as a function of the dimensionless coordinate x at angle $\theta=0$ for $M_H=M_W$. (a) The dashed, dotted, and solid curves represent the mixing angles $\theta_w=1.55$, $\theta_w=1.56$, and $\theta_w=1.565$, respectively. (b) For the U(1) gauge field function $F_7(x,\theta)$; dashed curve: mixing angle $\theta_w=1.55$, dotted curve: mixing angle $\theta_w=1.56$, solid curve: mixing angle $\theta_w=1.565$.

For the polynomial expansion we have been able to achieve a high numerical accuracy over the whole range of values of the mixing angle $0\leq\theta_w\leq\pi/2$, but we had to limit ourselves to expansions of order $l\leq 6$. For the direct integration of the *partial* differential equations we have been able to achieve a high numerical accuracy only for values of the mixing angle up to $\theta_w\leq 1.567$, and not all the way to the limiting value $\theta_w=\pi/2$. Thus the interesting questions of what the limiting sphaleron solution looks like and whether it has a finite energy remain open.

While at vanishing mixing angle $\theta_w=0$ the energy density of the sphaleron is spherical, it becomes spheroidal for finite values of the mixing angle. Equal density contours, represented by ellipsoids, become elongated in the z direction, and the ratio of major and minor half-axes increases with increasing mixing angle.

As the energy density deforms more and more strongly, the total energy of the sphaleron decreases with increasing mixing angle. The larger the mixing angle the faster this decrease becomes. At the physical value of the mixing angle, $\theta_w=0.5$, the energy has decreased only by about 1% compared to the spherical case. At $\theta_w=1.0$ and $\theta_w=1.5$ it has decreased by about 4% and 14%, respectively, and even at $\theta_w=1.567$, our largest reliable value, the energy has only decreased by about 17%. This relative weak dependence of the energy on the mixing angle is seen throughout the considered range of values of the Higgs-boson mass, $\frac{1}{2}M_W\leq M_H\leq 10M_W$.

Solutions of nonlinear equations, when considered as functions of an external parameter, often exist only up to a critical value of this parameter, where a bifurcation is encountered. Because of this phenomenon extrapolations for such solutions must be regarded with caution. In the case of the sphaleron with as external parameter the mixing angle we have not encountered a critical point beyond which the solution ceases to exist. On the contrary, the sphaleron has continuously deformed throughout the full range of this parameter, $0\leq\theta_w<\pi/2$. In fact, the estimate of Klinkhamer and Manton [6] of the effect the finite physical value of the mixing angle would have on the sphaleron has turned out to be remarkably good.

All previous calculations on baryon-number violation in the early Universe [7–10] have applied the spherical approximation of the electroweak sphaleron, neglecting the effects of the finite physical value of the mixing angle. Our analysis has shown that this approximation is very good, as far as the classical solution is concerned. We expect that also the analysis of the normal modes of oscillation around the true electroweak sphaleron solution will differ little from the analysis around the spherical, approximate solution [9,15,19,20]. We therefore expect that the previous calculations and conclusions on

baryon-number violation in the early Universe [7–10] will remain valid, at least with respect to the spherical approximation of the electroweak sphaleron employed there.

Since nonlinear systems often hold surprises, however, a definite conclusion on this very important aspect clearly requires performing the mode analysis around the axially symmetric sphaleron. After all, new instabilities of the sphaleron and associated new classical solutions might arise as the mixing angle increases from the spherical limit to the physical value and beyond.

Note added. Our numerical calculations indicate that the *hedgehog gauge* and the *physical gauge* are not appropriate for solving the equations of motion for the sphaleron at nonzero mixing angle (except for the zeroth-order polynomial expansion). In these gauges several of the functions F_i are not well defined at the origin, implying a diverging energy density at the origin. This phenomenon (absent in the case $\theta_w = 0$) will be discussed in a subsequent publication [21].

ACKNOWLEDGMENTS

One of us (J.K.) gratefully acknowledges discussions with G. 't Hooft, L. Wilets, and L. Yaffe and support from the Netherlands Organization for Scientific Research (NWO) and the Institute for Nuclear Theory (INT), Seattle.

[1] G. 't Hooft, Phys. Rev. Lett. **37**, 8 (1976).
[2] S. L. Adler, Phys. Rev. **177**, 2926 (1969); J. S. Bell and R. Jackiw, Nuovo Cimento **60**, 47 (1969); W. A. Bardeen, Phys. Rev. **189**, 1848 (1969).
[3] *Baryon Number Violation at the SSC?,* Proceedings of the Sante Fe Workshop, Sante Fe, New Mexico, 1990, edited by M. Mattis and E. Mottola (World Scientific, Singapore, 1990).
[4] A. Ringwald, Nucl. Phys. **B330**, 1 (1990).
[5] N. S. Manton, Phys. Rev. D **28**, 2019 (1983).
[6] F. R. Klinkhamer and N. S. Manton, Phys. Rev. D **30**, 2212 (1984).
[7] V. Kuzmin, V. Rubakov, and M. Shaposhnikov, Phys. Lett. **155B**, 36 (1985).
[8] P. Arnold and L. McLerran, Phys. Rev. D **36**, 581 (1987); **37**, 1020 (1988); L. Carson and L. McLerran, *ibid.* **41**, 647 (1990); L. Carson, Xu Li, L. McLerran, and R.-T. Wang, *ibid.* **42**, 2127 (1990).
[9] A. Ringwald, Phys. Lett. B **201**, 510 (1988); J. Kripfganz and A. Ringwald, Z. Phys. C **44**, 213 (1989).
[10] E. W. Kolb and M. S. Turner, *The Early Universe* (Addison-Wesley, Redwood City, CA, 1990).
[11] R. Dashen, B. Hasslacher, and A. Neveu, Phys. Rev. D **10**, 4138 (1974).
[12] B. Kleihaus, J. Kunz, and Y. Brihaye, Phys. Lett. B **273**, 100 (1991).
[13] N. S. Manton, Nucl. Phys. **B135**, 319 (1978).
[14] J. Kunz and Y. Brihaye, Phys. Lett. B **216**, 353 (1989).
[15] L. G. Yaffe, Phys. Rev. D **40**, 3463 (1989).
[16] C. Rebbi and P. Rossi, Phys. Rev. D **22**, 2010 (1980).
[17] F. R. Klinkhamer and R. Laterveer, Z. Phys. C **53**, 247 (1992).
[18] W. Schönauer and E. Schnepf, Parallel Computing **6**, 185 (1988).
[19] T. Akiba, H. Kikuchi, and T. Yanagida, Phys. Rev. D **40**, 179 (1989).
[20] Y. Brihaye and J. Kunz, Phys. Lett. B **249**, 90 (1990); Acta Phys. Pol. **93**, 513 (1992).
[21] J. Kunz, Y. Brihaye, and B. Kleihaus (in preparation).